

Unattended Sparse Acoustic Array Configurations and Beamforming Algorithms

M. R. Azimi-Sadjadi^{*a}, A. Pezeshki^b, L. L. Scharf^b, and G. Wichern^{b †}

^aInformation System Technologies, Inc.
Fort Collins, CO, 80521

^bElectrical and Computer Engineering Department
Colorado State University, Fort Collins, CO, 80523

ABSTRACT

Various sparse array configurations have been studied to improve spatial resolution for separating several closely spaced targets in tight formations using unattended acoustic arrays. To extend the array aperture, it is customary to employ sparse array configurations with uniform inter-array spacing wider than the half-wavelength intra-subarray spacing, hence achieving more accurate direction of arrival (DOA) estimates without using extra hardware. However, this larger inter-array positioning results in ambiguous DOA estimates. To resolve this ambiguity, sparse arrays with multiple invariance properties could be deployed. Alternatively, one can design regular or random sparse array configurations that provide frequency diversity, in which case every subarray is designed for a particular band of frequencies. These different configurations are investigated in this paper. Additionally, we present a Capon DOA algorithm that exploits the specific geometry of each array configuration. Simulation results are presented to study the pros and cons of different sparse configurations.

1. INTRODUCTION

Unattended passive acoustic sensors are widely used for remote battlefield surveillance, situation awareness and monitoring¹⁻⁴. These small and cost effective sensors can provide real-time information about different types of ground and airborne targets. They are rugged and reliable and can be left in the field for a long period of time after deployment. Generally, there can be a wide variety of target types in a battlefield depending on the specific mission, e.g. troops, ground targets (trucks, tanks, etc), airborne targets (helicopters, missiles, airplanes) with signatures that overlap both spectrally and temporally. Unfortunately, the existing DOA estimation algorithms have limited capability when applied to realistic multiple target scenarios, especially when the targets are spatially close together and move in tight staggered, abreast, or single-file formations. Additionally, performance is highly dependent on terrain, weather, and background noise estimates.

The spatial resolution may be improved by exploiting sparse array configurations^{5,6}. The existing sparse array processing methods are based on exploiting a shift invariance property between the array steering matrices of different subarrays in a sparse configuration. However, this invariance property is only valid when the distances between sources to the subarrays are far greater than the distances between the subarrays. It is only under such an assumption (further referred to as the far field assumption) that sparse processing can provide more accurate DOA estimates compared to the array processing on individual subarrays. However, as we will show in this paper, when the far field assumption is violated the accuracy of the DOA estimates obtained using the sparse processing algorithms degrade significantly.

Alternatively, we have proposed several other sparse configurations that exploit frequency diversity. In these configurations, sensors are deployed in regular or randomly scattered clusters, such that each cluster exploits a particular frequency band. Our experiments with these array configurations suggest that regularly or randomly deployed clusters of sensors that take advantage of frequency diversity can resolve closely spaced targets very accurately and at the same time are much less sensitive to near field effects. Interestingly, we have demonstrated that a sparse configuration consisting of 15 sensor elements (microphones) that are randomly deployed in an area

†no@infsyst.biz; phone: 1 970 224 2556; fax 1 970 224 2556.

^{*}A. Pezeshki, L. Scharf, and G. Wichern are consultants at Information System Technologies, Inc.

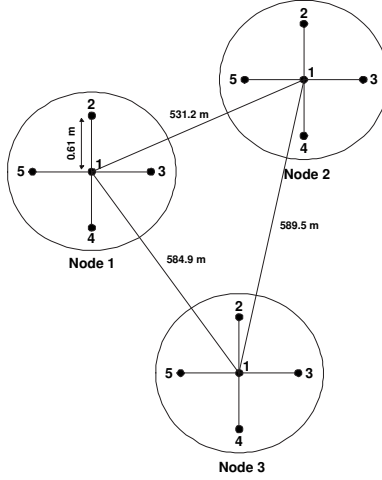


Figure 1. A sparse configuration with three 5-element wagon wheel subarrays.

as large as $150 \times 150m^2$ can produce more accurate DOA estimates and better resolve closely spaced sources than a sparse configuration consisting of three baseline 5-element wagon wheel arrays deployed in the same area.

Several studies are carried out to investigate DOA accuracy, target resolution, robustness to noise, and effects of sensor placement and array configurations on the beampattern and bearing response of the sparse array configuration. In these experiments, we have restricted our attention to synthetically generated narrowband sources, though the results and findings of this study can directly be applicable to wideband sources. For both Bartlett and Capon beamformers, the bearing responses of different array placement scenarios were studied. Additionally, specific experiments were conducted to identify technical issues and limitations in using sparse array methods, especially in scenarios where closely spaced near-field sources are present. These experiments are helpful in evaluating the performance of the sparse array methods as a function of range of the sources (near and far field) as well as the distance between the nodes. The results of these experiments may provide some guidelines on how to successfully design and deploy sparse arrays for the problem in hand.

2. SPARSE PROCESSING FOR ARRAYS WITH SHIFT INVARIANCE

In this section, we use the idea behind multiple invariance techniques^{5,6} in order to develop a sparse processing algorithm for the sparse configuration in Figure 1, which consists of three five-element wagon wheel subarrays. For the geometry in Figure 1, the array measurement vector for node i ($i = 1, 2$, and 3) at frequency f_j and over a fixed time snapshot may be expressed as

$$\mathbf{z}_i(f_j) = \mathbf{A}_i(f_j, \boldsymbol{\theta}_i)\mathbf{s}(f_j) + \mathbf{n}_i(f_j) \quad (1)$$

where $\mathbf{s}(f_j) = [s_1(f_j), \dots, s_d(f_j)]$ represents the vector of d narrow-band source signals at frequency f_j , $\mathbf{n}_i(f_j)$ is the measurement noise vector for node i at frequency f_j , and

$$\mathbf{A}_i(f_j, \boldsymbol{\theta}_i) = [\mathbf{a}_i(f_j, \theta_{i,1}), \dots, \mathbf{a}_i(f_j, \theta_{i,d})] \in C^{5 \times d} \quad (2)$$

is the array steering matrix for node i at frequency f_j that steers to d plane-waves at angles $\boldsymbol{\theta}_i = [\theta_{i,1}, \dots, \theta_{i,d}]^T$. Therefore, the l th steering vector of node i may be written as

$$\mathbf{a}_i(f_j, \theta_{i,l}) = [1, e^{j\frac{2\pi f_j r}{c} \sin(\theta_{i,l})}, e^{j\frac{2\pi f_j r}{c} \cos(\theta_{i,l})}, e^{-j\frac{2\pi f_j r}{c} \sin(\theta_{i,l})}, e^{-j\frac{2\pi f_j r}{c} \cos(\theta_{i,l})}]^T \in C^{5 \times 1} \quad (3)$$

where r is the radius of each wagon-wheel array and c is the speed of sound in air.

Assume that the sources are far field so that the angles at nodes 1, 2 and 3 are almost equal, i.e. $\boldsymbol{\theta} = \boldsymbol{\theta}_1 \approx \boldsymbol{\theta}_2 \approx \boldsymbol{\theta}_3$. This far field assumption is the fundamental assumption behind almost all sparse processing methods that are based on the idea of multiple invariance. Using this assumption and the geometry of the sparse array configuration in Figure 1, it may easily be shown that the array steering matrices at different nodes have the following translation invariance property:

$$\mathbf{A}_i(f_j, \boldsymbol{\theta}) = \mathbf{A}_1(f_j, \boldsymbol{\theta})\Phi_i(f_j, \boldsymbol{\theta}); \quad \text{for } i = 2, \text{ and } 3 \quad (4)$$

with $\Phi_i(f_j, \boldsymbol{\theta}) = \text{Diag}[e^{-j2\pi f_j(x_i \sin(\theta_1) + y_i \cos(\theta_1))} \dots e^{-j2\pi f_j(x_i \sin(\theta_d) + y_i \cos(\theta_d))}]$ where x_i and y_i are distances between node i to Node 1 along the x - and y -axis, respectively, assuming that Node 1 is positioned at the origin of the coordinate system.

Using this invariance property, we may define the augmented array steering matrix $\mathbf{A}(f_j, \boldsymbol{\theta})$, consisting of the array steering matrices of a subset or all the nodes, along with their corresponding augmented array measurement vector $\mathbf{z}(f_j)$. For the two node case, we can write

$$\mathbf{A}(f_j, \boldsymbol{\theta}) = \begin{bmatrix} \mathbf{A}_1(f_j, \boldsymbol{\theta}) \\ \mathbf{A}_i(f_j, \boldsymbol{\theta}) \end{bmatrix} = \begin{bmatrix} \mathbf{A}_1(f_j, \boldsymbol{\theta}) \\ \mathbf{A}_1(f_j, \boldsymbol{\theta})\Phi_i(f_j, \boldsymbol{\theta}) \end{bmatrix}; \quad \text{for } i = 2, \text{ or } 3 \quad (5)$$

and

$$\mathbf{z}(f_j) = [\mathbf{z}_1^H(f_j) \quad \mathbf{z}_i^H(f_j)]^H; \quad i = 2, \text{ or } 3 \quad (6)$$

The augmented measurement vector $\mathbf{z}(f_j)$ may be viewed as an array measurement vector recorded by an array with steering matrix $\mathbf{A}(f_j, \boldsymbol{\theta})$. In other words, $\mathbf{z}(f_j)$ and $\mathbf{A}(f_j, \boldsymbol{\theta})$ are regarded as the measurement vector and steering matrix for a single array, and hence all the standard beamforming and DOA estimation methods may be applied to them in order to estimate the angle $\boldsymbol{\theta} = [\theta_1, \dots, \theta_d]^T$. For example, we may use the Capon beamforming method⁷ to estimate the angles:

$$C(f_j, \theta_l) = \frac{1}{\mathbf{a}^H(f_j, \theta_l)\mathbf{R}_{zz}^{-1}(f_j)\mathbf{a}(f_j, \theta_l)} \quad (7)$$

where $\mathbf{a}(f_j, \theta_l)$ is the l th column of $\mathbf{A}(f_j, \boldsymbol{\theta})$, and $\mathbf{R}_{zz}(f_j)$ is the covariance matrix of $\mathbf{z}(f_j)$.

Note that for the wideband sources the power spectra at different frequencies may be averaged together to produce a wideband Capon⁷ bearing response. It has been shown⁸ geometric average of narrowband output powers provides more accurate DOA estimates compared to arithmetic and harmonic averages. Thus for the wideband case, we consider the following wideband Capon bearing response⁸

$$C(f, \theta_l) = \prod_{j=1}^J C(f_j, \theta_l) = \prod_{j=1}^J \frac{1}{\mathbf{a}^H(f_j, \theta_l)\mathbf{R}_{zz}^{-1}(f_j)\mathbf{a}(f_j, \theta_l)} \quad (8)$$

where J is the total number of narrowband frequency components.

2.1. Sparse Processing Results on Synthesized Data

In this section, we apply the sparse processing method of Section 2 to a synthesized data in order to study the performance of sparse arrays with respect to changes in the distance between the nodes in a specific configuration, the number of arrays, and ability to resolve closely spaced sources.

2.1.1. Study 1: Node Distance and DOA Accuracy

For the studies in this section, we consider two sparse nodes with wagon-wheel arrays of 5 microphones, where the center microphone of the first node is positioned at the origin of the coordinate system. We gradually increase the distance between the nodes, at several steps, by moving the second node apart from the first one, along the line (x -axis) that connects the center elements of the two nodes (arrays). At each step, the developed sparse array processing method is applied to estimate the DOA's. The synthesized data set contains a narrow-band

source at frequency 128Hz (mid-frequency 0-256Hz for most sources). The initial location of the source is at $[-700m, 1000m]$. The source moves along the y -axis at a constant speed of $-20m/sec$. The closest point of approach (CPA) of the source to Node 1 is 700m. The source signal is recorded by the two nodes for 80 seconds, with the sampling rate of 1024Hz. Random white Gaussian noise is added to the source signals at the SNR of 25dB.

Figures 2(a)-(e) show the DOA estimates obtained using the developed sparse processing method, when the distance between the two nodes were 7m, 21m, 48m, 276m, and 531m, respectively. In these plots, the solid lines show the true DOA's with respect to Node 1, and the dots show the estimates generated by the developed sparse algorithm. Looking at these figures, one can see that as the separation between the nodes increases the accuracy of the DOA estimates decreases. Note that in all these cases the source travels a similar path where the range of the source to Node 1 varies between 1200m to 700m. The reason being the far field assumption mentioned in Section 2 is no longer valid when the distance between the source and nodes is comparable with the distance between the nodes. When the far field assumption is violated, the translation invariance relation between the steering matrices of the nodes is no longer valid either. From these results it seems that, for a CPA of 700m, the case in which the nodes are 21m apart (Figure 2(b)) produces reasonable DOA estimates. The accuracy of DOA estimates in Figure 2(a), where the distance between the nodes is 7m, are very close to those in Figure 2(b). However, positioning the nodes too close together results in a small coverage area, and hence may not be cost effective.

The plot of the means and standard deviations of DOA estimation error as a function of distance between the nodes are shown in Figure 2(f). This plot is generated over the entire duration of the signal (80 sec.) and it clearly shows that when the distance between the nodes exceeds 21m, the standard deviation of the DOA error increases rapidly with the increase in distance owing to the fact that the fundamental far field assumption and hence the translation invariance property for sparse processing are no longer valid. In other words, when the distance between the nodes exceeds 21m the array steering matrices of the nodes are no longer related to each other via a simple diagonal translation matrix. As a matter of fact, the steering matrices will be dependent on more than one DOA vector. We emphasize that these results are obtained for a source that its CPA to the Node 1 is 700m.

2.1.2. Study 2: Sparse Array and Resolving Multiple Sources

In order to study the capability of the developed sparse processing method in separating closely spaced sources, another study is conducted in which the synthesized data consists of two narrow-band sources, both at frequency 128Hz. The two sources move in a single file formation with a constant speed of $-20m/sec$ along the y -axis. The distance between the nodes is chosen to be 21m, while the CPA of the sources to Node 1 is greater than or equal to 700m.

Figures 3(a),(c), and (e) show the DOA estimates for three different source separation, namely 100m, 50m, and 30m, obtained using Node 1 array alone (no sparse processing). Figures 3(b),(d), and (f), on the other hand, show the DOA plots for these three cases obtained using the sparse processing method of Section 2 with two nodes of separation 21 m. Looking at Figure 3(a), we see that for the first 20 seconds, where the angular separation between the two sources is small, the single node Capon algorithm is not able to resolve the two sources. However, as shown in Figure 3(b) using the sparse array one can successfully resolve the two sources during this period of time. In Figures 3(c) and (e) where the separation between the sources is 50 and 30 meters, respectively, the single node Capon algorithm does not resolve the two sources at any time. However, in the corresponding plots for sparse processing method, i.e. Figures 3(d) and (f), the tracks of the two sources are successfully resolved, at almost all snapshots, except at the very beginning of the plots where the angular separation between the sources is very small. The plot in Figure 3(f) shows that the developed sparse processing method can resolve two sources which their angular separation is even as close as 2 degrees! We must note that the angular resolution also depends on the type of the beamforming method that is employed with the sparse processing.

The results in this section show that when the far field assumption is satisfied, the sparse processing algorithms provide higher resolution than the single node DOA estimation algorithms and can resolve closely spaced targets that are not resolvable by the single node algorithms.

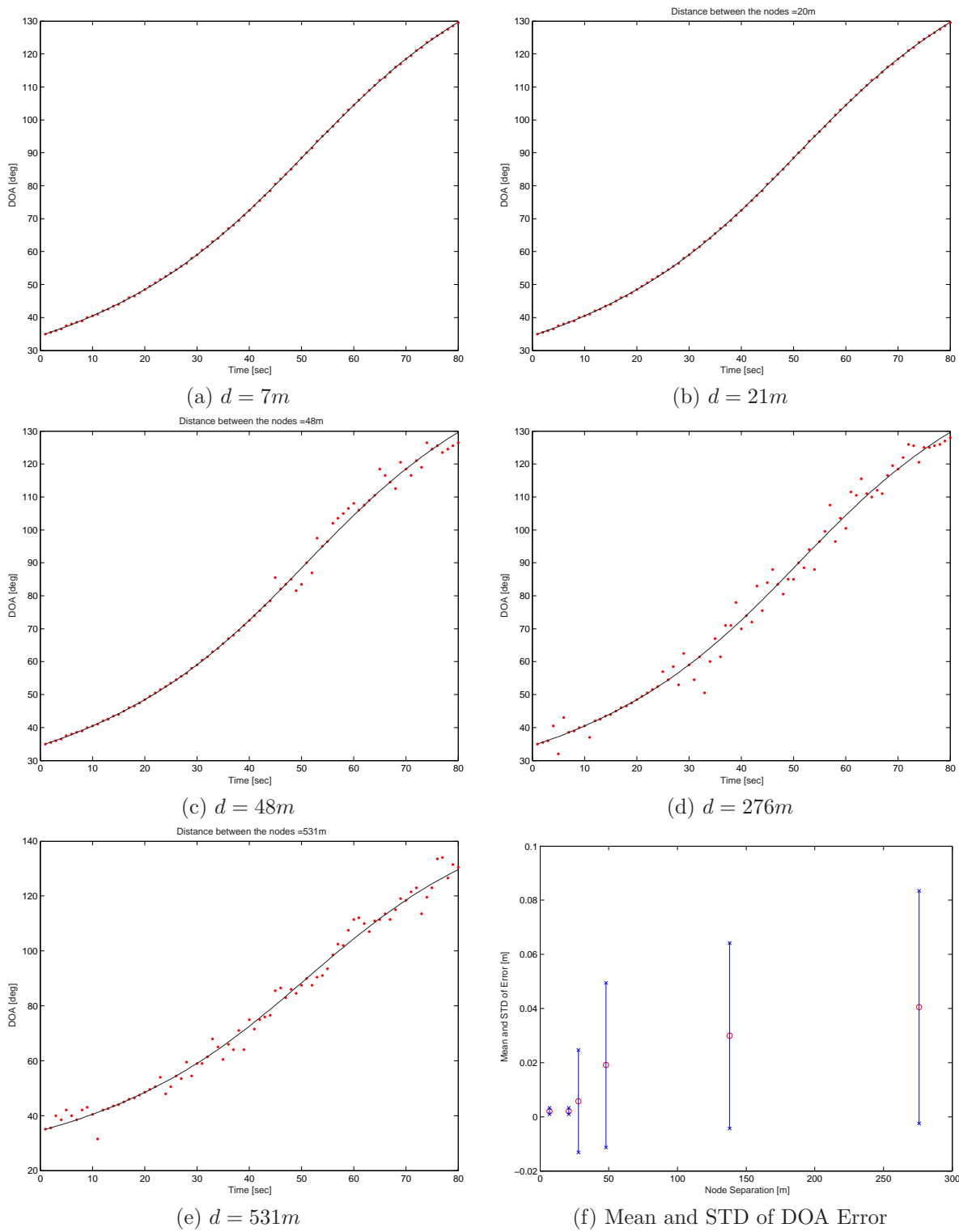
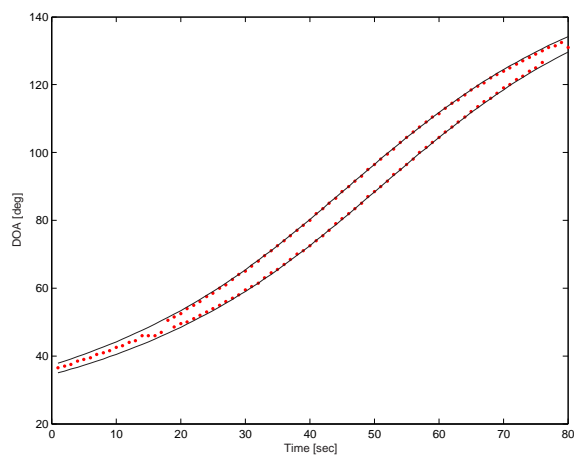
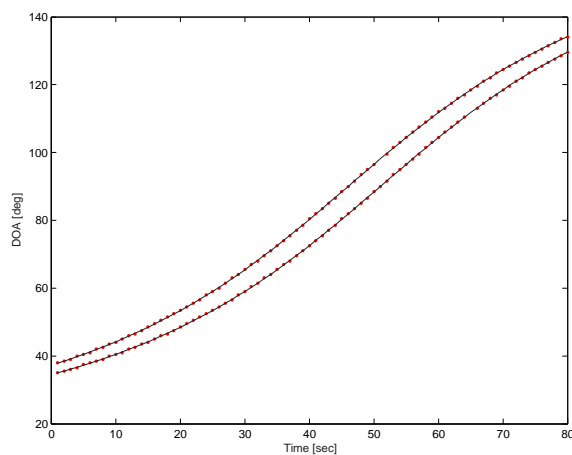


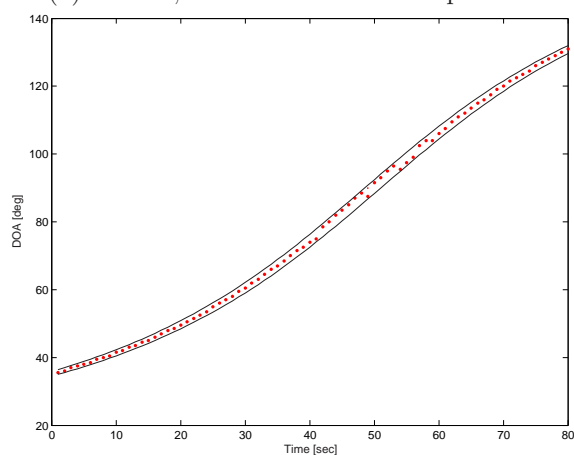
Figure 2. Studying the performance of the developed sparse processing method as a function of node separation.



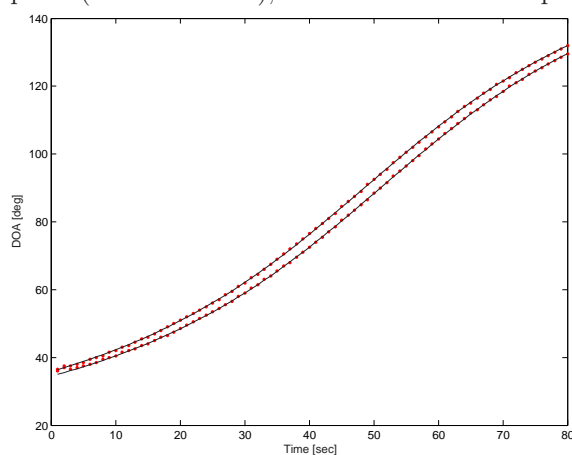
(a) Node 1; 2 source with 100m separation



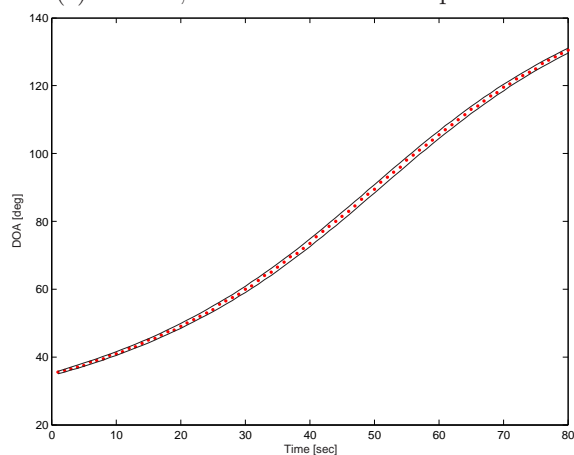
(b) Sparse (Nodes 1 and 2); 2 source with 100m separation



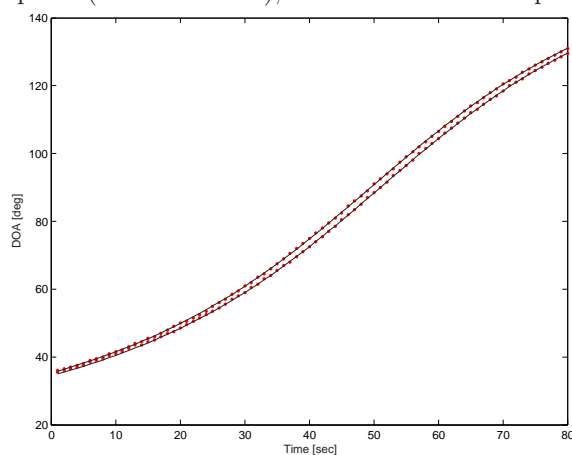
(c) Node 1; 2 source with 50m separation



(d) Sparse (Nodes 1 and 2); 2 source with 50m separation



(e) Node 1; 2 source with 30m separation



(f) Sparse (Nodes 1 and 2); 2 source with 30m separation

Figure 3. Studying the angular resolution of the developed sparse processing method.

2.2. Optimizing the Sparse Array Configuration

In this section, we investigate how the placement of multiple arrays in a sparse configuration can affect the beamforming performance. In particular, we are interested to see how a sparse configuration should be devised in order to minimize the side-lobes in the bearing responses and beampatterns of Capon and Bartlett beamformers.⁷ For this purpose, we consider a narrow-band wavefront with wavelength λ , arriving at an angle of $\pi/2$ rad (broadside). The arrays are 5-element wagon-wheel-type with radius of $\lambda/2$. We consider two identical wagon-wheel arrays, where the position of one of them is fixed at the center of the coordinate system. The second array can slide along the line that connects the center of the two arrays. By changing the distance between the two arrays from $d = 2\lambda/2$ to $d = 9\lambda/2$, in $\lambda/2$ increments, we produce several two-array sparse configurations. In each case, we determine the bearing responses of (two-array) sparse Bartlett and Capon beamformers. The questions we intend to address are: (a) can we attenuate the side-lobes by carefully positioning multiple arrays in a sparse configuration?; and (b) can we improve resolution of the main-lobe?

To study the beampattern and bearing response of the Bartlett beamformer⁷ for two-node sparse array, let us denote the look angle by θ and the true angle of a single source by ϕ . The steering vector for the 5-element array is $\mathbf{a}_1(f, \theta)$ where f is the narrowband frequency. The received signal for a narrowband source of frequency f is $\mathbf{x}_1(f, \phi)$. The covariance matrix of the received signal can be written as $\mathbf{R}_{\mathbf{x}_1\mathbf{x}_1} = E[\mathbf{x}_1\mathbf{x}_1^H]$. Assuming signal and noise variances of σ_s^2 and σ_{n1}^2 , respectively, the output power the Bartlett beamformer for a single array is,

$$G_1(\theta, \phi, f) = \mathbf{a}_1^H \mathbf{R}_{\mathbf{x}_1\mathbf{x}_1} \mathbf{a}_1 = \sigma_s^2 |\mathbf{a}_1^H \mathbf{s}_1|^2 + \sigma_{n1}^2 = B_1^{1/2} B_1^{H/2} + \sigma_{n1}^2 \quad (9)$$

where $\mathbf{s}_1(f, \phi)$ is the narrowband source vector and $B_1 := B_1^{1/2} B_1^{H/2}$, with $B_1^{1/2} := \sigma_s \mathbf{a}_1^H \mathbf{s}_1$, is the output power of the noise-free Bartlett beamformer. Now for a sparse array of two identical 5-element arrays with certain separation the combined steering vector can be written as $\mathbf{a}_2(f, \theta) = [\mathbf{a}_1^H(f, \theta) \quad \mathbf{a}_1^H(f, \theta)e^{-j\psi_2}]^H$ where $\psi_2(\theta)$ represents the translation angle between the two arrays for the look angle θ . This follows from the structure in (4) for the steering matrix. Also, the combined signal vector impinging on the sparse array may be expressed as $\mathbf{s}_2(f, \phi) = [\mathbf{s}_1^H(f, \phi) \quad \mathbf{s}_1^H(f, \phi)e^{-j\varphi_2}]^H$ where $\varphi_2(\phi)$ represents the true translation angle between the two arrays for the true angle ϕ . If we assume that the noise variance in the received signal of the second array is σ_{n2}^2 , then it can easily be shown that the output power of the sparse Bartlett beamformer is,

$$\begin{aligned} G_2(\theta, \phi, f) &= \mathbf{a}_2^H \mathbf{R}_{\mathbf{x}_2\mathbf{x}_2} \mathbf{a}_2 = G_1 + B_1 + 2B_1 \cos(\varphi_2 - \psi_2) + \sigma_{n2}^2 \\ &= 2B_1(1 + \cos(\psi_2 - \varphi_2)) + \sigma_{n1}^2 + \sigma_{n2}^2 \end{aligned} \quad (10)$$

Remark: This result can be extended to p subarrays. In this case, the combined steering vector can be written as $\mathbf{a}_p(f, \theta) = [\mathbf{a}_{p-1}^H(f, \theta) \quad \mathbf{a}_1^H(f, \theta)e^{-j\psi_p}]^H$ where $\psi_p(\theta)$ represents the translation angle between the sparse array consisting of $p-1$ arrays and the p^{th} array for the search direction θ . Also, the combined signal vector impinging on the sparse array can be expressed as $\mathbf{s}_p(f, \phi) = [\mathbf{s}_{p-1}^H(f, \phi) \quad \mathbf{s}_1^H(f, \phi)e^{-j\varphi_p}]^H$ where $\varphi_p(\phi)$ represents the true translation angle between the sparse array consisting of $p-1$ arrays and the p^{th} array for the true angle ϕ . Then, the output power of the sparse Bartlett beamformer becomes

$$G_p(\theta, \phi, f) = \mathbf{a}_p^H \mathbf{R}_{\mathbf{x}_p\mathbf{x}_p} \mathbf{a}_p = G_{p-1} + B_1 + 2\text{Re}\{B_{p-1}^{1/2} B_1^{H/2} e^{j(\psi_p - \varphi_p)}\} + \sigma_{np}^2 \quad (11)$$

Also, we can show that

$$B_{p-1}^{1/2} = B_{p-2}^{1/2} + B_1^{1/2} e^{j(\varphi_{p-1} - \psi_{p-1})} \quad (12)$$

These two recursive equations can be used to efficiently compute the output power of the sparse Bartlett beamformer for a sparse array consisting of p identical nodes (e.g. circular or linear arrays). For sparse Capon beamformer similar approach can be taken.

Figures 4(a)-(i) compare the bearing responses of the single-array Bartlett (Figure 4(a)) and the two-array sparse Bartlett beamformers, for various distances between the two arrays. As expected, the main-lobes of the bearing responses occur at the look direction of $\pi/2$ rad, as the actual arriving angle is $\pi/2$ rad. Comparing these

main-lobes with the main-lobe of the single-array Bartlett beamformer (Figure 4(a)), it seems that in the sparse case the main-lobe is just a “modulated version” of the main-lobe in the single node case, where the frequency of the modulating signal increases as the distance between the two nodes increases. By “modulated version” we mean that the main-lobe in the sparse case is the product of the main-lobe in single node case and some periodic function. This is shown in (10) that the bearing response of the two-array sparse Bartlett is related to the bearing response of a single array Bartlett by a function of cosine of the delay between the two arrays. Another interesting observation is that for the cases where the distance between the two arrays is an even multiple of the half-wavelength $\lambda/2$ (Figures 4(b),(d),(f), and (h)) the side-lobe at look direction of 0 rad is large, whereas for the cases where the distance between the arrays is an odd multiply of $\lambda/2$ (Figures 4(c),(e),(g), and (i)) this side-lobe is attenuated significantly.

The above observations about the modulation of the main-lobe and attenuation of side-lobes may also be made for the bearing responses of the (two-array) sparse Capon beamformer, which are shown in Figures 5(b)-(i). Similar to the Bartlett case, the wavefront is arriving at angle $\pi/2$ rad, and the distance between the two arrays is varied from $d = 2\lambda/2$ to $d = 9\lambda/2$, in $\lambda/2$ increments. As can be seen, the sparse Capon beamformer indeed improves the resolution of the main-lobe when compared with the single array case (Figure 5(a)) with the price of increasing the ambiguity due to large number of side-lobes, especially at longer separation. Also, when the distance between the arrays is an even multiply of $\lambda/2$ (Figures 5b),(d),(f), and (h)) the side-lobe at the look direction of 0 rad is relatively large, whereas for cases where the distance between the two arrays is an odd multiply of $\lambda/2$ (Figures 5(c),(e),(g), and (i)) this side-lobe is considerably attenuated. The variability of the side-lobe structure to the distance between the nodes is clearly evident from these results. These results suggest that by carefully positioning multiple arrays in an sparse configuration, it is possible to reduce the side-lobes at certain look directions and concentrate the power at the true arriving angle.

3. SPARSE ARRAY CONFIGURATIONS WITH FREQUENCY DIVERSITY

The results in the previous section showed some of the main problems with sparse array configurations that possess invariance properties. Clearly, the main idea behind multiple invariance^{5,6} arrays is to take advantage of various microphone spacings some of which are less than one-half wavelength of the source signal while the others are greater than one-half wavelength. In this way, for those groups of microphones that have spacings less than one-half wavelength of the source signal, coarse but unambiguous DOA estimates can be produced; whereas the sparsely located sub-arrays provide fine resolution for the DOA estimates at the cost of introducing ambiguity in form of the grating lobes. Thus, by combining both properties, the unambiguous coarse DOA estimates may be used to eliminate the ambiguities introduced by aliasing. However, as shown in the previous section, this invariance property becomes invalid for near field sources hence leading to poor DOA estimation results. Moreover, the variability of the side-lobe structure with the distance between the nodes becomes a major issue when there are uncertainties in the locations of the arrays/microphones. There are various other configurations that can be employed to accurate DOA estimates for closely spaced targets without these problems. The following studies introduce other possible configurations that exploit frequency diversity and offer very promising characteristics.

3.1. Study 1: Multi-Ring Array Configurations

To fully utilize different subarrays that work for specific frequency bands, we devise a regular three-ring sparse array where the inner ring has 8 elements, the middle ring has 6 elements and the outer ring has 4 elements. With this configuration, we have 4 circular array possibilities covering frequency subbands 246, 123, 92 and 41 Hz and 2 linear subarrays that cover frequency bands 193 and 96 Hz. Thus, this configuration with 19 microphones gives great frequency diversity and it does not suffer from the aliasing effects, since each important subband has its own subarray. This multi-ring array provides more accurate DOA estimates depending on range and frequency band. Moreover, this configuration does not have the deficiencies of the sparse arrays that exploit multiple invariance properties, especially for near field DOA estimation when invariance is no longer valid.

To show the usefulness of this sparse configuration, an experiment is conducted where a two-ring array of 15-microphones was designed to separate two narrowband sources with frequency $f = 128\text{Hz}$, at SNR of 15dB.

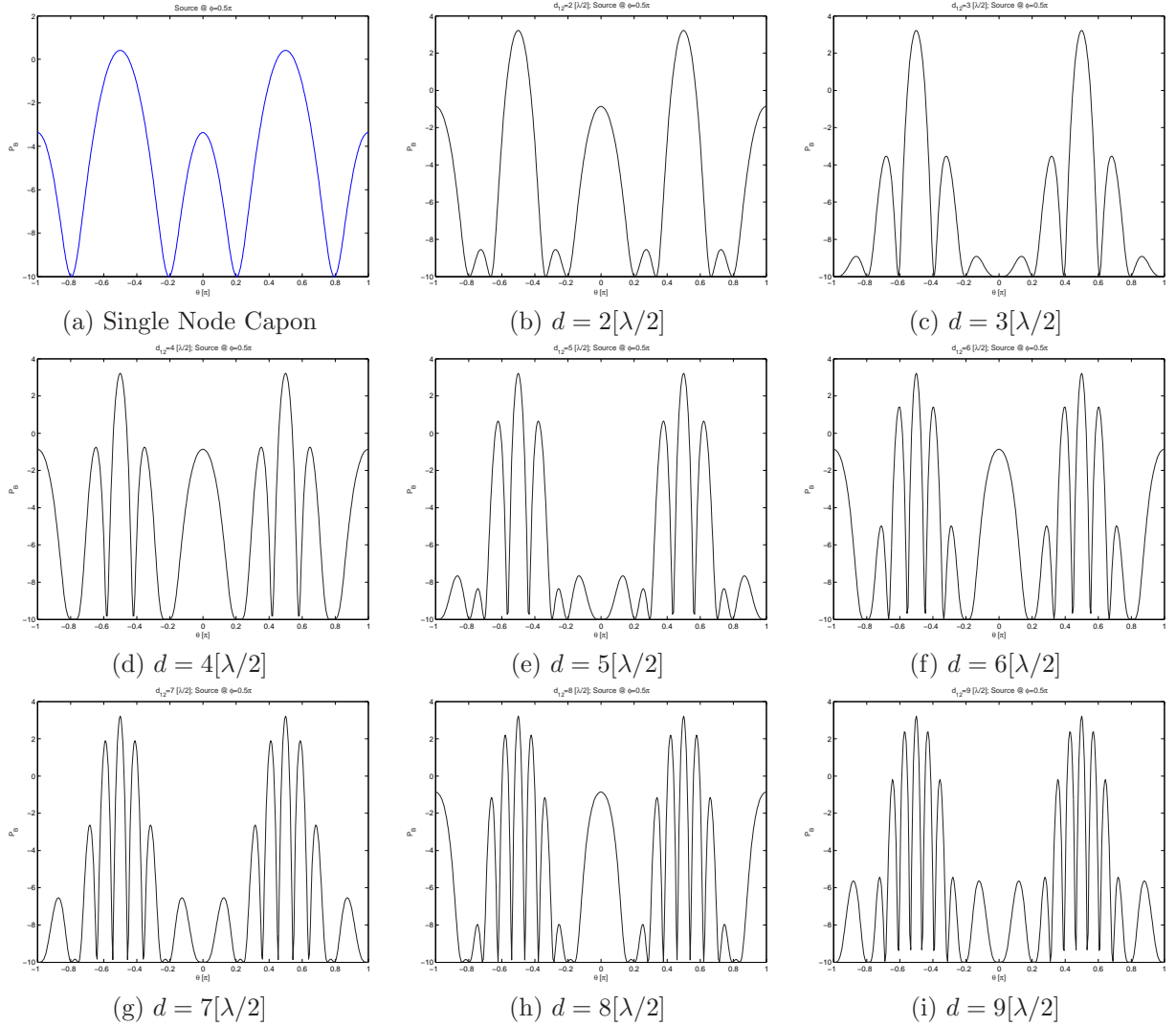


Figure 4. Bearing responses of the (two-array) sparse Bartlett beamformer to source at $\pi/2$ rad (broadside).

The inner and outer rings (radii of .88 and 1.76m) consisted of 8 and 6 elements, respectively. The sources are 50m apart and move from NE to SW at a constant speed of -10m/sec and -15m/sec along x -axis and y -axis, respectively. Figure 6(a) shows the DOA estimates generated using this two-ring array, while Figure 6(b) gives the DOA estimates generated using three 5-element wagon wheel arrays with 2ft radius, separated by 50 and 100m from the center element of the first node. Although, both array configurations use 15 microphones, the DOA accuracy of the two-ring array is by far better than that of the regular baseline arrays. The inaccuracy of the latter structure can be attributed to non-optimal spacings of the nodes (see Study 1 in Section 2.1.1), bad grating lobe structure of this configuration, and near field effects. The only shortcoming of this two-ring array is the difficulty to design and deploy such a relatively large array. Thus, the questions that arise here are: (a) Can we construct randomly scattered arrays that offer frequency diversity via multiple tight and sparse clusters of microphones? (b) How do they perform comparing to regular structures? These questions are addressed in the next section.

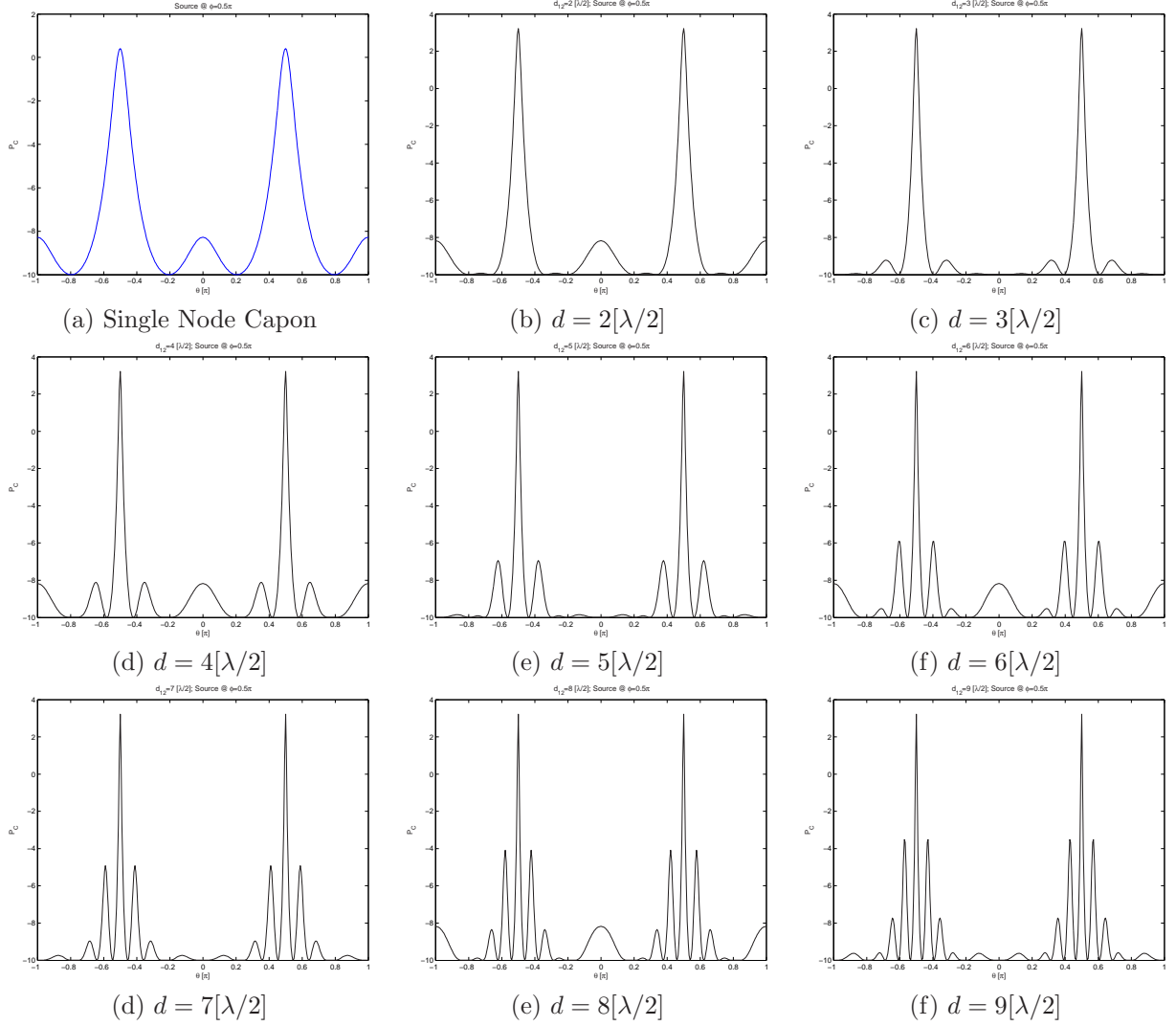
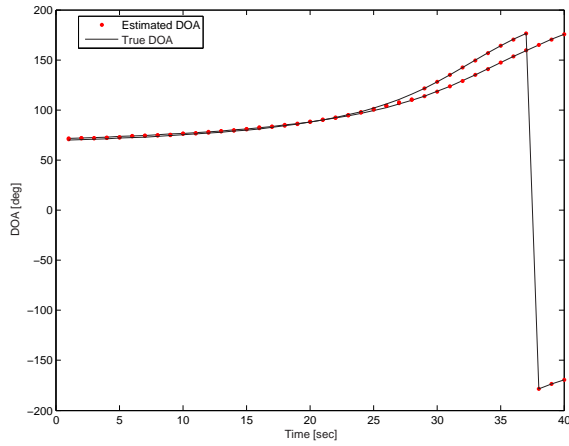


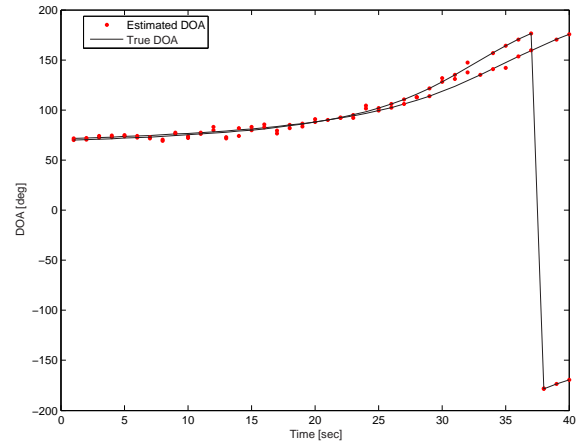
Figure 5. Bearing responses of the (two-array) sparse Capon beamformer to source at $\pi/2$ rad (broadside).

3.2. Study 2: Sparse Arrays of Randomly Scattered Single Microphones

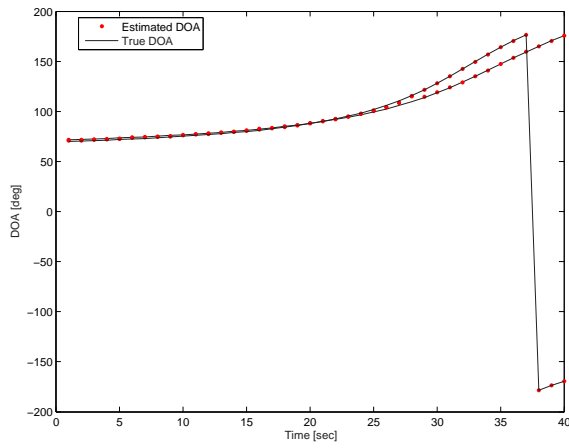
In this experiment, random placement of single microphones is considered. Here, we can either try to cluster the microphones in some randomly perturbed version of the two-ring configuration with approximately the same coverage area or randomly distribute them in a larger area taking into account our clustering needs in terms of subband coverage and frequency diversity. Figure 6(c) shows the DOA estimates of the perturbed two-ring array where a random perturbation with standard deviation of 20% of the radius was introduced. Comparing to the results in Figures 6(a) and (b), it is interesting to note that the accuracy is not much sacrificed by this random placement. Figures 6(d)-(f), on the other hand, show the results of the randomly scattered microphones forming an inner and outer cluster with 6 and 9 elements and much bigger perturbed radii of $(r_1, r_2) = (25, 75m)$ for (d), $(r_1, r_2) = (25, 125m)$ for (e), and $(r_1, r_2) = (25, 175m)$ for (f), respectively. These cases correspond to area coverage of $150 \times 150m^2$, $250 \times 250m^2$, and $400 \times 400m^2$, respectively. These results reveal some intriguing properties and the potential of this new paradigm of deploying single microphones in a relatively large surveillance area. Obviously, even for $250 \times 250m^2$ coverage the randomly scattered two cluster arrays outperform the three baseline array structure. This is primarily due to the fact that the random array does not suffer from



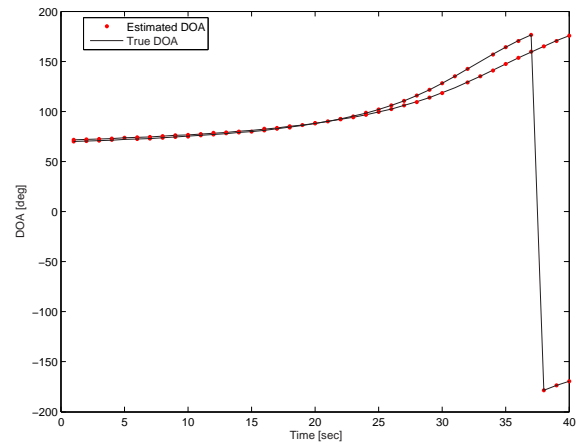
(a) Two-ring array.



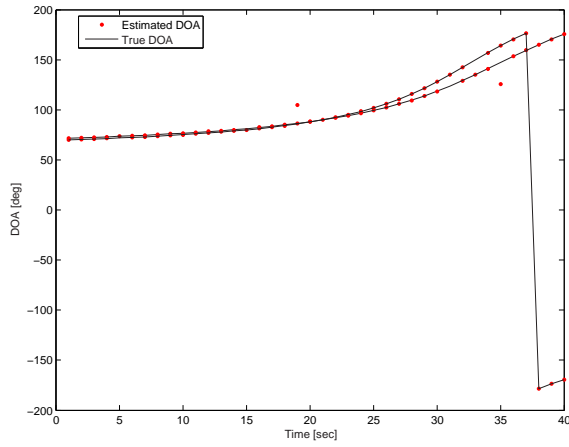
(b) Three 5-element baseline arrays.



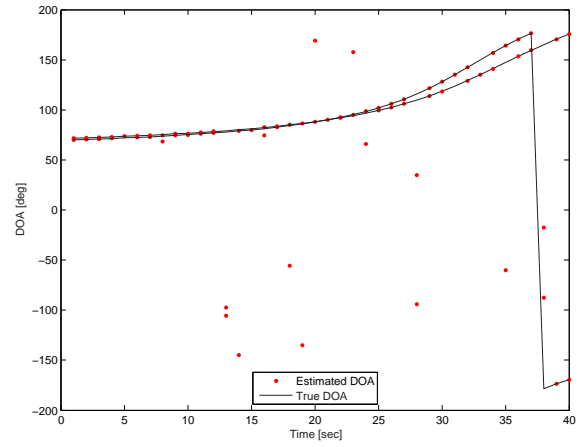
(c) Perturbed two-ring.



(d) Randomly scattered clusters ($150 \times 150m^2$)



(e) Randomly scattered clusters ($250 \times 250m^2$)



(f) Randomly scattered clusters ($400 \times 400m^2$)

Figure 6. DOA accuracy of different regular and randomly scattered two-ring/cluster arrays.

the grating lobe structure of the regular baseline arrays and further it is not sensitive to near field effects.

4. CONCLUSIONS

Several sparse array configurations were considered and the pros and cons of each configuration were investigated. More specifically, the performance of the conventional sparse processing configurations, which exploit the invariance property, were studied. It was shown that when the distances between the sources and the subarrays are far greater than the distances between the subarrays (far field assumption) the conventional sparse processing methods offer good performance and resolve closely spaced sources. When the far field assumption is violated the DOA accuracy dramatically deteriorates in these structures.

Alternative sparse configurations were also proposed, in which sensors were distributed in regular or random fashion to construct sparse clusters of sensors. For these configurations each cluster of sensors exploits a particular frequency band. Our experiments suggest that randomly deployed clusters of microphones provide better resolution in separating multiple closely spaced targets and at the same time are less sensitive to near field effects. Our results on synthetic narrowband sources indicate that a randomly scattered sparse configuration consisting of 15 microphones could potentially provide very good DOA accuracy even in a surveillance area of approximately $250 \times 250m^2$. These observations must be validated on real sparse array data.

ACKNOWLEDGMENTS

This work is funded by Army SBIR-Phase II contract # DAAE30-03-C-1055. The data and technical support has been provided by the US Army TACOM-ARDEC, Picatinny Arsenal, NJ. The authors would like to thank Bob Wade and Myron Hohil at Picatinny Arsenal, NJ for their invaluable suggestions and technical support.

REFERENCES

1. N. Srour, "Unattended ground sensors- a prospective for operational needs and requirements," *ARL Report Prepared for NATO*, October 1999.
2. T. Pham and M. Fong, "Real-time implementation of MUSIC for wideband acoustic detection and tracking," *Proc. of SPIE AeroSense'97: Automatic Target Recognition VII*, Orlando, FL, April 1997.
3. T. Pham and B. M. Sadler, "Wideband array processing algorithms for acoustic tracking of ground vehicles," *ARL Technical Report*, Adelphi, MD, 1997.
4. M. R. Azimi-Sadjadi, "Detection, tracking and classification of multiple targets using advanced beamforming and classification methods: phase II," *First-Year Summary Report, Phase II SBIR-Army*, January 2004.
5. K. T. Wong and M. D. Zoltowski, "Direction finding with sparse rectangular dual-size spatial invariance array," *IEEE Trans. on Aerospace Electron. Syst.*, vol.34, pp. 1320-1327, October 1998.
6. M. D. Zoltowski and K. T. Wong, "Closed-form eigenstructure-based direction finding using arbitrary but identical subarrays on a sparse uniform Cartesian array grid," *IEEE Trans. on Signal Processing*, vol. 48, pp. 2205-2210, Aug. 2000.
7. H. L. Van Trees, *Optimum Array Processing*, Wiley Interscience, 2002.
8. M. R. Azimi-Sadjadi, A. Pezeshki, L. Scharf, and M. Hohil, "Wideband DOA estimation algorithms for multiple target detection and tracking using unattended acoustic sensors," *Proc. of the SPIE'04 Defense and Security Symposium.*, Vol. 5417, pp. 1-11, Orlando, FL, April 2004.